Chapter 2
Equilibrium Pathway of Ultrathin Polymer Films as Revealed by Their Surface Dynamics

Kun Geng, Fei Chen, Zhaohui Yang and Ophelia K.C. Tsui

Abstract The majority of thin polymer films are prepared by spin-coating. In spin-coating, a drop of polymer solution is spread into a film which then dries into a solid in less than a minute. Abruptness of this process is believed to leave the polymer chains insufficient time to equilibrate, causing them to be kinetically trapped in an intermediate, transitory state. Indeed, several out-of-equilibrium attributes have been unequivocally identified, including residual stress, reduced chain entanglement and on-going polymer adsorption to the substrate surface. Upon annealing above the glass transition temperature, T_g, these attributes evolve toward equilibrium. Another important, though less discussed out-of-equilibrium attribute is the smoother-than-equilibrium surface structure of as-cast spin-coated polymer films. Because of this, these films usually roughen upon heating. Importantly, the roughening process, especially for nanometer films, often results in the formation of deep holes and thereby ultimate rupture of the films. A question then naturally arises as to whether evolutions in the residual stress, chain entanglement and polymer adsorption may interfere with the roughening process, whereby modify the film stability. In recent years, our group has developed methods to monitor and analyze the surface roughening process. By applying these methods, important physical properties such as the effective viscosity and shear modulus of the films have been deduced. In this chapter, we shall briefly review these methods and the

K. Geng · F. Chen · O.K.C. Tsui (✉)
Department of Physics, Boston University, Boston, MA 02215, USA
e-mail: okctsui@bu.edu

O.K.C. Tsui
Division of Materials Science and Engineering, Boston University, Boston, MA 02215, USA

Z. Yang
Center for Soft Condensed Matter Physics and Interdisciplinary Research, Soochow University, Suzhou 215006, People's Republic of China

Z. Yang
College of Physics, Optoelectronics and Energy, Soochow University, Suzhou, China

S. Napolitano (ed.), *Non-equilibrium Phenomena in Confined Soft Matter*,
Soft and Biological Matter, DOI 10.1007/978-3-319-21948-6_2

respectively model analyses. On the basis of these discussions, we then deliberate whether or not evolutions in the chain entanglement density, residual stress and adsorption phenomenon in the films may have influenced the roughening process measured, and thereby project their impacts on the film stability.

2.1 Introduction

Polymers are large molecules made of repetition of the monomer unit. The resultant large molecular mass renders polymers unique properties such as toughness and viscoelasticity. These, together with their relatively low-cost and abundance in variety, have made polymer the material of choice in a myriad of applications. As new technologies are introduced to enable the manufacturing of ever smaller devices, the past two decades have witnessed a rapid growth in the use of polymer nanometer films.

Spin-coating is a prevalent method for making polymer nanometer films. During spin-coating, a drop of polymer solution is deposited on a substrate surface, which is then spun at $\sim$500 to $\sim$4000 rpm. The rapid spinning causes the solution to spread and dry into a solid film. Such a process, typically completes in less than a minute, is believed to be too rapid for the polymer chains to equilibrate before the film vitrifies. As a result, polymers in spin-coated films are frequently cited to be out-of-equilibrium [1]. Supposition as such has been exploited to explain some of the more bizarre results, such as negative thermal expansivity [2–5] and existence of a large residual stress comparable to the rubbery elastic modulus of the bulk polymer [6–8]. More recent experiments also found that polymer chains are prone to adsorb irreversibly onto solid substrates. Moreover, the slow process by which it takes place can cause certain dynamic responses to take a prohibitively long time to attain equilibrium [9–13]. A number of effective methods have been developed to diagnose and understand the out-of-equilibrium properties of spin-coated polymer films, as one may readily see by browsing through this book. In this chapter, we shall focus on the equilibrium pathway of the films as revealed by the evolution of their surface. As noticed early on, the surface profile of as-cast spin-coated polymer films is usually smoother than equilibrium [2]. As a result, these films roughen when they are heated above the T_g [14]. An illustration is given in Fig. 2.1, which compares the power spectral densities (PSDs) of a spin-coated polystyrene (PS) film before and after annealing at $\sim$20 °C above the bulk T_g for $\sim$2 h. Evidently, the PSD grew notably upon annealing, which signifies roughening. By examining how the common out-of-equilibrium attributes of spin-coated films, such as residual stress, reduced chain entanglement and chain adsorption to the substrate surface, correlate with the roughening process, one may gain insight about whether or not the out-of-equilibrium attributes modify the film stability.

This chapter is organized as follows. In the next section (Sect. 2.2), we describe how PSDs like the ones shown in Fig. 2.1 are measured. In Sect. 2.3, we discuss the

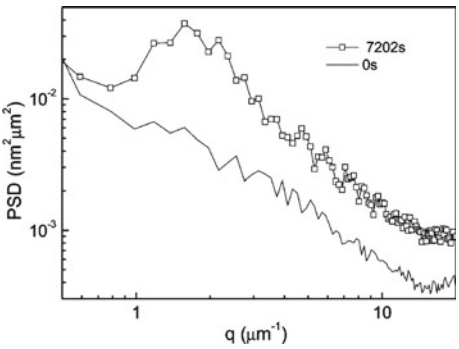

Fig. 2.1 Power spectral density of an h_0 = 18 nm and M_w = 2.3 kg/mol spin-cast polystyrene film, freshly prepared (*plain solid line*) and after annealing for 7202 s (open squares) at 85 °C (Reproduced with permission from Ref. [13])

theoretical models we developed to analyze the time-varying PSDs whereby the effective viscosity and effective shear modulus of the films can be determined. In addition, we also discuss how the information hence obtained may be used to infer the density of chain entanglement and other properties of the films that may affect the transport processes. In Sect. 2.4, we discuss how by exploiting any temporal variation in the effective viscosity and shear modulus or lack thereof in our measurements, one may infer information about the out-of-equilibrium state of the films. Finally, we conclude this chapter with a summary of the major observations.

2.2 Experimental Method

Experimentally, we determine the dynamics a film by studying how its power spectral density (PSD) evolves with time upon annealing at a given measurement temperature. To determine the PSD, we first measure the surface topography of the films by using tapping-mode atomic force microscopy (AFM). Then we convert each topographic data (a 2-dimensional image) to its PSD (a 1-dimensional array) [15–18] by first multiplying it by a Welch function then Fourier-transforming it [15–18]. The resulting two-dimensional Fourier spectrum is then radial averaged to produce the one-dimensional PSD.

It is important to clarify that the present AFM measurement is fundamentally different from most other AFM measurements used for materials characterization [19–23]. In typical AFM measurements [19, 23], the AFM probe tip actively perturbs the specimen surface and thereafter monitors the dynamic response *local* to the film surface. Because the size of the probe tip is often quite small (typically $< \sim 10$ nm), even a small probing force can translate into a large stress (e.g. for a force of 0.1 nN, the stress is ~ 1 MPa) that can result in non-linear response for

soft materials like polymer. But in our method, the AFM probe tip acts as a *passive*, benign monitor (through the use of light and high-frequency tapping) of the surface topography of the film as the film surface roughens spontaneously by thermal activation. Although our method measures the surface dynamics of the film (namely the dynamics by which the film surface evolves), it will become apparent in Sect. 2.3 that the measured dynamics arises from flow transport of *all* the materials in the film and so should reflect an overall dynamics. That being said, one may still be able to infer information about the local dynamics at the free surface by applying a layer model to the measurement as discussed in the next Section.

It should also be clarified that the dynamics we measure can differ from that inferred from experiments involving capillary action of a solid substrate or wall, such as dewetting (more specifically, holes opening) or wicking of the polymer liquid into an empty capillary [24–28]. In contrast, our measurement is based on thermally activated dynamics, where the driving stress, σ, (neglecting the conjoining pressure due to the interfacial potential) is due to gradient in the Laplace pressure, $\Delta P \sim 2\gamma/R$, arising from undulations in the film surface. (Here, $\gamma \approx 30$ mN/m is the surface tension and R is the local radius of curvature of the undulating film surface.) For undulations with amplitude δh and wavevector q, $R \sim 1/(q^2 \delta h)$. Adopting the experimental condition, $\delta h < 0.1 h_0$ (see below) and for $h_0 = 10$ nm, $\sigma \sim \gamma \delta h q^2 <\sim 30$ Pa. But in the experiments involving capillary action, the stress is provided by the polymer-substrate surface tension and given by $\sigma = \gamma/h_0$. As pointed out by Reiter [26], $\gamma \sim 20$ to 30 mN/m and so for $h_0 \sim 10$ nm, the stress is ~ 2 to 3 MPa and large enough to cause plastic deformation of thin films of common polymers such as polystyrene. Indeed, spectacular phenomena had been observed in these experiments, including molecular layering of the precursor film of a polymer liquid spreading on a solid substrate [29] and formation of a highly asymmetric rim on the periphery of an enlarging hole in a viscoelastic (entangled) polymer film [26]. The latter should be contrasted with the relatively symmetric holes rims found in situations where there is no capillary action—a condition realized when the holes only appear as indentations, and have not yet grown deep enough to touch the substrate surface (see Fig. 2.11).

As we shall discuss in the next section, the dynamics we measure can be succinctly characterized by the effective viscosity of the film, η_{eff} [30]. In general, the value of η_{eff} varies with measurement time and does not reach the steady-state value until a sufficiently long time [15–18]. In any given measurement, a priori we do not know how long it will take η_{eff} to reach the steady-state value. To ensure that the steady-state value is reached, we continue the measurement until the measured η_{eff} no longer change when the annealing time is lengthened four times or more. Because our analysis is based on linear approximations [31], measurements are only taken in the initial stage of roughening where the root-mean-square roughness is less than $0.1 h_0$, where h_0 is the average film thickness.

2.3 Model Analysis for the Temporal Evolution of Power Spectral Density

2.3.1 *Analysis for the Surface Dynamics of Newtonian Liquid Films*

In this subsection, we shall discuss the model we developed to describe the surface dynamics of unentangled polymer films, which we treat as Newtonian liquids.

For a film possessing small undulations on its surface, the height profile can be written as $h(\boldsymbol{r}) = h_0 + \delta h(\boldsymbol{r})$, where h_0 is the average film height, $\boldsymbol{r}$ denotes positions in the plane of the film and $<\delta h(\boldsymbol{r})>_{\boldsymbol{r}} = 0$. The presence of $\delta h(\boldsymbol{r})$, whether spontaneously [32–34] or artificially created [35–37], produces a spatially inhomogeneous excess pressure according to $\Delta P(\boldsymbol{r}) = -\gamma\nabla^2\delta h(\boldsymbol{r}) + dG(h_0)/dh$ [17, 38], where γ is the surface tension and $G(h)$ the van der Waals potential of the film. Given this, the pressure gradient, ∇P, is generally nonzero, causing the film fluid to flow, which in turn produces temporal variations in $\delta h(\boldsymbol{r})$ and $P(\boldsymbol{r})$ (Here, $P(\boldsymbol{r}) = P_{\text{atm}} + \Delta P(\boldsymbol{r})$, where P_{atm} is the atmospheric pressure.) In the lubrication approximation, where the in-plane length scale of the undulations is much bigger than h_0, the unit-width, in-plane current is given by $\boldsymbol{j}(\boldsymbol{r}, t) = -M_{\text{tot}}\nabla P(\boldsymbol{r}, t) + \xi(\boldsymbol{r}, t)$ [31], where M_{tot} denotes the mobility and $\xi(\boldsymbol{r}, t)$ conserved thermal noise. It should be remarked that inclusion of thermal noise in the treatment is essential for yielding good agreement with experiment [39].

By applying linear analysis, the following expression for the time-varying PSD, $A_q^2(t)$, was derived [2, 16, 30, 31, 40, 41]:

$$A_{\boldsymbol{q}}^2(t) = A_{\boldsymbol{q}}^2(0)\exp(2\Gamma t) + \left[\frac{k_B T}{d^2G(h_0)/dh^2 + \gamma q^2}\right](1 - \exp(2\Gamma t)) \tag{2.1a}$$

where

$$\Gamma(\boldsymbol{q}) = -M_{\text{tot}}\left[(d^2G(h_0)/dh^2)q^2 + \gamma q^4\right]. \tag{2.1b}$$

In here, $\boldsymbol{q}$ is the wavevector and $q \equiv |\boldsymbol{q}|$, k_B is the Boltzmann constant, T is absolute temperature. Figure 2.2a, b, respectively, shows a sequence of AFM images and corresponding PSDs acquired from a representative low molecular weight (M_w) PS film. The solid lines in Fig. 2.2b represent the best fit to (2.1a). As one can see, the model is able to describe the data well.

If the no-slip boundary condition applies at the substrate surface and the film viscosity is homogeneous and given by η, one may derive that [31]

$$M_{\text{tot}} = h_0^3/(3\eta). \tag{2.2}$$

The mobility M_{tot} defined here is analogous to the proportionality constant, $\pi R_0^4/(8\eta)$ found in the Poiseuille equation (i.e., $dV/dt = [\pi R_0^4/(8\eta)]\nabla P$), which relates

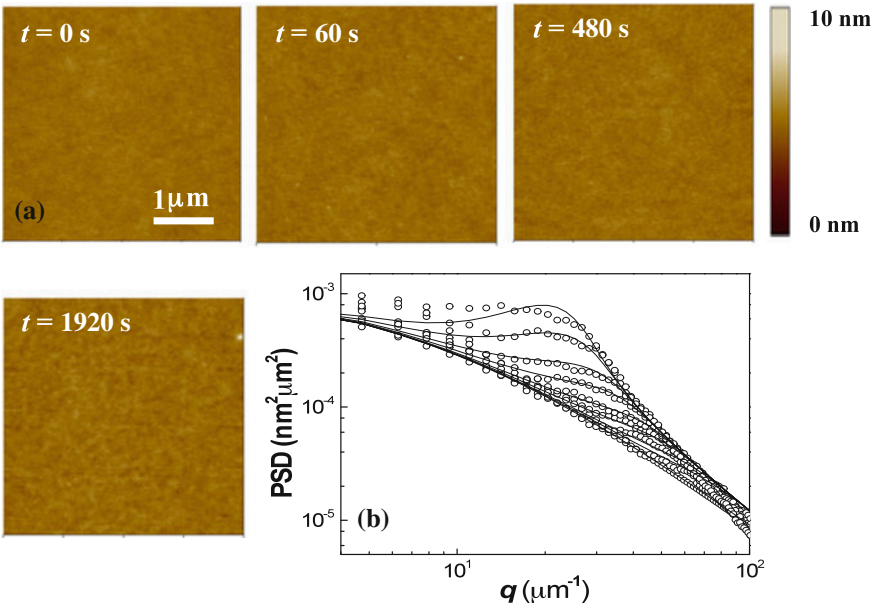

Fig. 2.2 A representative sequence of atomic force microscopic (AFM) topographic images and power spectral density we obtained. The data was taken from a film with initial thickness, $h_0 = 4$ nm and $M_w = 2.4$ kg/mol annealed at 61 °C. **a** A subset of the AFM images. **b** The full set of power spectral, PSD, of the film at times (from *bottom* to *top*): 0, 15, 30, 60, 90, 210, 600, 1080, 2100, 3840 and 7200 s (*open circles*). The *solid lines* are the best fit to (2.1a) (Reproduced with permission from Ref. [43])

the fluid current engendered by applying a pressure gradient across a fluid-filled cylindrical pipe with radius R_0 and non-slipping wall [42]. One may observe that this mobility follows the pipe dimension to the power 4, but $M_{tot} \sim h_0^3$ in (2.2). The different power laws arise from the fact that the current considered in the Poiseuille equation is the volumetric fluid flow rate (dV/dt, m^3/s) through the entire cross-section of the cylindrical conduit, but that considered in thin films ($\boldsymbol{j}(\boldsymbol{r}, t)$, m^2/s) is the fluid flow rate per unit width of the film cross-section. Given the above expression of M_{tot}, it is common to define the effective viscosity as follows [30, 31]:

$$\eta_{eff} \equiv h_0^3/[3M_{tot}]. \tag{2.3}$$

In general, the dynamics and hence local viscosity in the film may not be uniform. In fact, more often than not the region near the polymer-air surface has a lower local viscosity [44] than the rest of the films [30]. Assuming the mobility of the near-air surface to be M_{mobile} and the viscosity of the rest of the film to be bulk-like and given by η_{bulk}, it has been shown that $M_{tot} \approx M_{mobile} + h_0^3/(3\eta_{bulk})$ for polymer films [43, 45, 46]. In the presence of dynamic heterogeneity as such, the value of η_{eff} obtained from (2.3) would be an effective viscosity, which explains the

subscript "eff" attributed to the symbol η_{eff}. Experiments performed on thick ($h_0 \geq \sim 80$ nm) low-M_w polystyrene supported by silica (PS-SiO_x) and poly(methyl methacrylate) supported by silica (PMMA-SiO_x) had found good agreement between the measured η_{eff} and bulk viscosity [2, 43, 47, 48]. These agreements confirm the present method for viscosity measurement. They also indicate that any effects of enhanced surface mobility [2, 35, 43, 47, 48] or interfacial slippage are insignificant in these films.

2.3.2 *Analysis for the Surface Dynamics of Viscoelastic Films*

To develop a model for analyzing the surface dynamics of entangled polymer films, which are viscoelastic (and so not Newtonian), we use an adiabatic approximation described as follows [31]. Figure 2.3 depicts a representative sequence of PSDs obtained from an entangled polymer film upon annealing above the T_g from the as-cast state for various times t as indicated in the figure legend (open symbols). After the first annealing time step (namely from t = 0–640 s, Fig. 2.3), the PSD shows an abrupt jump. This jump is caused by the glass-to-rubber transition, and not treated in our model. After this jump, there is a lengthy period of time of about 22400 s or 6.2 h where the PSDs show insignificant growth. Even though the PSDs show little growth in this time, frame-to-frame comparison between the PSDs acquired in separate, in situ measurements showed that the surface topography of the film was actually not stationary. This indicates that the film was in a quasi-steady state, undergoing equilibrium vibrations. We attribute the vibrations to the normal modes of the film in the rubbery elastic state. After t = 22400 s, the

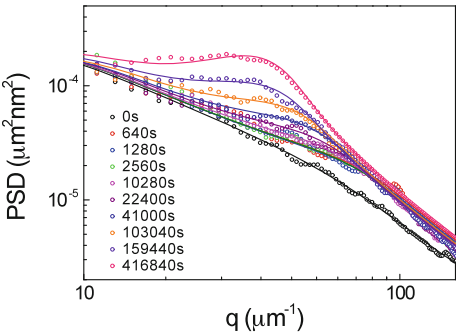

Fig. 2.3 Power spectral density of a h_0 = 3 nm, M_w = 115 kg/mol PS film upon annealing at 115 °C for various times as shown in the legend (*open circles*). The *solid lines* are model lines obtained by fitting the data to (2.4a), which gives $\eta_{eff,0} \equiv h_0^3/(3M_{tot}) = 4.2 \times 10^8$ Pas and μ_0 = 10 kPa (Reproduced with permission from Ref. [41])

growth of the PSDs becomes apparent again (Fig. 2.3). Therefore, there are two dynamic processes with different time scales, corresponding to the fast vibrations associated with the initial "stagnant PSD regime" and the slow dynamic process associated with the later stage where the growth of the PSDs becomes visible. Adopting an adiabatic approximation, we analyzed slow evolution of the film surface or PSD in the presence of the ensemble-averaged quasi-equilibrium fast vibrations [31]. We ascribe the slow evolution to the in-plane transport currents $\boldsymbol{j}(\boldsymbol{r}, t)$ caused by the local pressure gradient $\nabla P(\boldsymbol{r}, t)$ as discussed in the last section. For the fast vibrations, we assume the energy of the modes to be $[3\mu_0/(2h_0^3q^2)]|u_{\mathbf{q}}|^2$, in accord with that of the surface vibrations of an elastic film with wavevector $\boldsymbol{q}$, amplitude $u_{\mathbf{q}}$, and shear modulus μ_0 [49]. A linear calculation assuming lubrication approximation ($qh_0 << 1$) and stable films gives [31]:

$$A_{\boldsymbol{q}}^2(t) = A_{\boldsymbol{q}}^2(0)\exp(2\Gamma' t) + \left[\frac{k_B T}{d^2G(h_0)/dh^2 + \gamma q^2}\right](1 - \exp(2\Gamma' t)) \tag{2.4a}$$

where

$$\Gamma'(\boldsymbol{q}) = -M_{\text{tot}}q^2\left[\left((d^2G(h_0)/dh^2) + \gamma q^2\right)^{-1} + \left(\frac{3\mu_0}{h_0^3q^2}\right)^{-1}\right]^{-1}. \tag{2.4b}$$

The solid lines in Fig. 2.3 are model lines obtained by fitting the data to (2.4a). As one can see, the model lines are able to simultaneously capture the stagnant PSD and subsequent PSD growth regimes, and also provide a good description to the data.

On writing $M_{\text{tot}} = h_0^3/(3\eta_{\text{eff},0})$ as in (2.2), where $\eta_{\text{eff},0}$ denotes the effective viscosity of the film in the slow or growing PSD regime, we observe that the expression of $\Gamma'(\boldsymbol{q})$ in (2.4b) becomes identical to that derived by Safran and Klein [50] for a uniform Maxwell liquid film with no slip. This demonstrates consistency of our model with the Maxwell liquid model. However, we emphasize that in deriving (2.4a) and (2.4b), little assumption had been made about the slow process, and certainly no assumption had been made about whether there is dynamic homogeneity or interfacial slippage in the film. The only attribute we had assumed of the slow process is the generic relation, $\boldsymbol{j}(\boldsymbol{r}, t) = -M_{\text{tot}}\nabla P(\boldsymbol{r}, t)$. As a result, the value of M_{tot} or equivalently the steady-value of η_{eff} we measure (we measure) should be open to interpretation.

As mentioned in Sect. 2.2, in each measurement we do not know beforehand when the slow process is fully established and has reached the steady state. To ensure that the steady state of the slow process has been reached, we continue the measurement until further increase in the measurement time causes no change to the fitted value of M_{tot} and hence η_{eff}. To illustrate this, we fit the PSDs displayed in Fig. 2.3 one-by-one to (2.1a) and (2.1b) and deduce η_{eff} then plot the result as a function of annealing time t in Fig. 2.4 by solid circles. There, one sees that η_{eff} establishes the steady-state value after $t > \sim 20000$ s. The fact that the steady-state

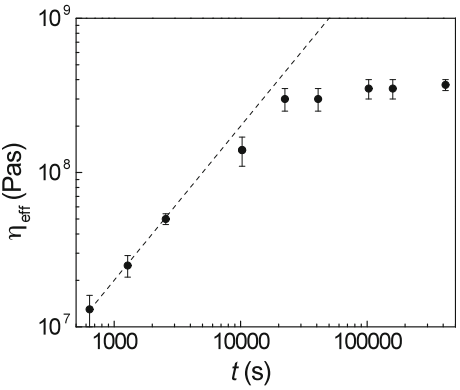

Fig. 2.4 Values of η_{eff} obtained by fitting the PSDs in Fig. 2.3 one-by-one to (2.1a, 2.1b), plotted versus the annealing time, t. The *dashed line* is a plot of $\eta_{eff} = 2\mu_0 t$ (Reproduced with permission from Ref. [41])

value ($\sim 4 \times 10^8$ Pas, Fig. 2.4) is consistent with the value obtained above by fitting the data directly to (2.4a, 2.4b) (Fig. 2.3) affirms our measurement protocol for determining the steady-state η_{eff}.

We summarize this subsection by recapitulating that we have derived (2.4a, 2.4b), which are able to simultaneously describe the short-time stagnant and long-time PSD growth regimes. In deriving these equations, the short-time (fast) dynamics is assumed to be caused by the normal modes of the films in the rubbery elastic state. For the long-time (slow) dynamic process, the only assumption that has been made is the general relation, $\boldsymbol{j}(\boldsymbol{r}, t) = -M_{tot}\nabla P(\boldsymbol{r}, t)$. With this, a steady-state effective viscosity may be defined as before, namely $\eta_{eff,0} \equiv h_0^3/(3M_{tot})$. In the case of thick PS-SiO_x, a previous experiment [2] showed that the value of $\eta_{eff,0}$ is the same as the bulk viscosity of the polymer, indicating that dynamic inhomogeneity and slippage can be ignored in these films. However, in cases where dynamic inhomogeneity or slippage cannot be ignored, $\eta_{eff,0}$ is an effective viscosity and can depend on the film thickness in general. In such circumstances, further analysis of the $\eta_{eff,0}(h_0)$ dependence would be necessary to pinpoint the origin of the slow process.

2.4 Factors Contributing to the Out-of-Equilibrium State

In this section, we discuss how our measurement may or may not reflect the three factors commonly attributed to the out-of-equilibrium state of thin polymer films, namely reduced entanglement density, residual stress and on-going chain adsorption to the substrate surface.

2.4.1 Reduced Entanglement Density

As discussed above, due to the abruptness of the spin-coating process, some memories of the polymer chain conformation in the original polymer solution may get carried over to the final dry film. One common speculation is that spin-coated films may inherit the lower degree of entanglement the polymer chains have in the solution state just before vitrifying [51, 52]. This proposition gains support from the experiment of Barbero et al. [52], who studied the viscosity of spin-coated PS-SiO_x ($h_0 \geq \sim$ 100 nm) before and after thermal annealing. For the unentangled films ($M_w < M_e \approx$ 18 kg/mol [53]), they found that the unannealed and annealed films both exhibited the bulk viscosity. But for the entangled films (c.f. M_w = 113 and 655 kg/mol), the unannealed films exhibited reduced viscosity as though the entanglement density of the as-cast films was lower than equilibrium. With annealing, the viscosity of the films increased, but the extent to which the bulk value was recovered differed for different M_w's. For M_w = 113 kg/mol, the recovery was complete, but for M_w = 655 kg/mol it was partial.

As Fig. 2.4 shows, our measurements of the entangled films also exhibit temporal variation in the value of η_{eff}. Specifically, η_{eff} first increases linearly with time then reaches the steady-state value, $\eta_{eff,0}$ after a characteristic time, τ_r. For the films with $h_0 > 4R_g$, we had previously found that the value of $\eta_{eff,0}$ agrees with the bulk viscosity [2]. Moreover, the characteristic time increases with M_w [2]. These observations are in keeping with the observations of Barbero et al. [52]. But as discussed below, interpretation of this data may not be straightforward. Sometimes, if not most times, it is more appropriate to estimate the rubbery-state shear modulus μ_0 from the data and then the density of entanglement, ρ_e, by using the relation, $\mu_0 = \rho_e RT = \rho RT/M_e$ [54], where ρ is mass density. As discussed below, the values of μ_0 we measure show that ρ_e is $\sim$1/10 times the equilibrium value.

For $t < \tau_r$, the films are in the rubbery elastic state. According to Fredrickson et al., the PSD of an elastic film with shear modulus μ_0 and no slip at the substrate surface is given by [49]:

$$A_q^2(t) = \text{Background} + \frac{k_B T}{d^2 G(h_0)/dh^2 + \gamma q^2 + \frac{3\mu_0}{h_0^3 q^2}}, \tag{2.5}$$

where "Background" refers to the low-q segment of the PSD corresponding to the surface modes with relaxation times longer than the measurement time t and so have not been able to evolve yet [2]. Separately, the expression for the liquid-film PSD (2.1a) can be written in the following approximated form [2]

$$A_q^2(t) = \text{Background} + \frac{k_B T}{d^2 G(h_0)/dh^2 + \gamma q^2 + \frac{3(\eta_{eff}/2t)}{h_0^3 q^2}}. \tag{2.6}$$

During the rubbery elastic regime, the films are elastic so (2.5) should apply. But on reaching the slow dynamic regime, (2.6) should apply. A comparison between (2.5) and (2.6) indicates that if we fit the data in the elastic regime to (2.1a), we should find that the fitted value of η_{eff} increases linearly with t, with the constant of proportionality equal to $2\mu_0$. Clearly, this prediction is supported by the short-time data of Fig. 2.4. By fitting this data to $\eta_{eff} = 2\mu_0 t$ (dashed line, Fig. 2.4), we obtain $\mu_0 = 10$ kPa. We remark that this value of μ_0 is consistent with the one we obtained by fitting the PSDs directly to (2.4a, 2.4b). We have applied this analysis to the PS-SiO_x films with M_w = 115 kg/mol [41] and 212 kg/mol [40] and h_0 = 2 to 125 nm, and found that the values of μ_0 agree with 10 kPa within a factor of 2. Since the bulk value of μ_0 is also independent of M_w and ≈100 kPa [55], this implies a $\sim$10 times reduction in μ_0.

Now we interpret the meaning of the noted reduction in μ_0. First, we discern that the linear t dependence seen in our η_{eff} measurement (Fig. 2.4) should not be interpreted "literally", meaning that the data should not be interpreted as being caused by the as-cast film already in the viscous flow regime with an effective viscosity that increased linearly with t. To this end, we examine the η_{eff} versus t data taken from the h_0 = 125 nm PS-SiO_x films with M_w = 212 kg/mol at various temperatures, T, between 130 and 160 °C (Fig. 2.5). Since our earlier experiment showed that for thick films as such the steady-state effective viscosity $\eta_{eff,0}$ agrees with the bulk viscosity, η_{bulk} [2], the reptation model should apply to these films. According to the reptation model, the viscosity and reptation time is $\eta \sim M_e^{-2}$ and $\tau_{rep} \sim M_e^{-1}$, respectively [2]. In Fig. 2.5, one observes that the value of η_{eff} acquired at the shortest time accessible to experiment ($t \approx 10$ s) is always about the same ($\sim 2 \times 10^5$ Pas) and independent of T. The steady-state viscosity $\eta_{eff,0}$ ($\equiv \eta_{eff}(t \rightarrow \infty)$), on the other hand, shows a strong T dependence following that of η_{bulk}, as expected [48]. So, a "literal" interpretation of the $\eta_{eff}(t)$ data in Fig. 2.5 would mean that the entanglement molecular weight of the as-cast films, $M_e' = M_e$

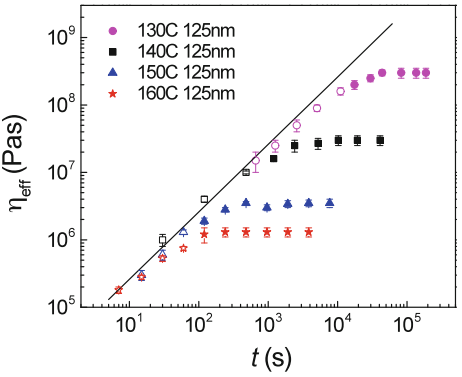

Fig. 2.5 Effective viscosity η_{eff} versus time obtained from PS-SiO_x films with h_0 = 125 nm films annealed at various temperatures between 130 and 160 °C. The *solid line* is a plot of $\eta_{eff} = 2 \times (10.5\ \text{kPa}) \times t$ (Data reproduced with permission from Ref. [40])

$[\eta_{eff}(t \rightarrow \infty)/\eta_{eff}(t \approx 10\ s)]^2$ varies between $\sim$25 and 2.2×10^6 times the equilibrium M_e. This is clearly not physical since all the films were prepared in the same way. On the other hand, the data of all these films show the same linear t-dependence before reaching the steady-state value. Adopting the interpretation that the linear t dependence is due to the films being in the elastic-state or stagnant PSD regime for which $\eta_{eff} = 2\mu_0 t$, this observation implies that the films exhibit the same shear modulus μ_0 independent of the measurement temperature T. But a constant value of μ_0 is expected in here since $\mu_0 = \rho RT/M_e$ and T varies by less than $\sim$7% in Fig. 2.5. This confirms the latter interpretation for a linear $\eta_{eff}(t)$ dependence, namely it corresponds to the films being in the elastic dynamic regime, with a measured value of μ_0 equal to $\sim$1/10 times the equilibrium value. It should be underlined that the "literal" interpretation of $\eta_{eff}(t)$ cannot be excluded in general. It is excluded here only because of the data shown in Fig. 2.5 as discussed above. Invalidation (or validation) of the literal interpretation has yet to be examined for polymer films spin-cast from a θ solvent [56].

A simple explanation for the 10 times reduction in μ_0 would be that the entanglement molecular weight is increased to $\sim 10M_e$ in the as-cast films. In the final stage of spin-coating, the concentration of polymer in the film (while still a solution) increases and the chain dynamics slows down. As the volume fraction of the polymer in the film reaches a large enough value, say ϕ^*, the chain conformation may be kinetically frozen in. One may estimate the value of ϕ^* as follows. Assuming $M_e(\phi^*) = M_e(1)(\phi^*)^{-1.3}$ for polymer in an athermal solvent (see p. 370 of [54]), $\mu_0 = \mu_{0,equilibrium}(M_e(1)/M_e(\phi^*))$ and $\mu_0/\mu_{0,equilibrium} = 1/10$, we may deduce that $\phi^* = 17$ %. We observe [40] that this is close to the volume fraction where chain overlap begins to occur inside an athermal solvent (n.b. $\phi_e \approx [M_e(1)/M_w]^{0.76} = [17\ k/212\ k]^{0.76} = 15$ %; see p. 369 of [54].), but much smaller than the volume fraction (≈80 % [57]) where a PS/toluene solution (which is the solution used here) vitrifies at room temperature. We find such a result for the estimated value of ϕ^* reasonable. It is because changes in the entanglement density M_e' should be viable only by chain motions with length scales at least on the order of the instantaneous tube size; the motions associated with the glass transition, being on the segmental length level, are too local to be relevant. All being said, we should however caution that the value of μ_0 is derived from (2.5), which assumes the no slip boundary condition. If slippage cannot be ignored, it may also constitute a cause for the measure μ_0 to be smaller than the bulk value.

Next, we ponder the possibility of observing recovery of the entanglement density in this experiment, if it takes place. As discussed above, glass-to-rubber transition occurs in the first time step of heating, causing the PSD to jump to the rubbery elastic PSD. Correspondingly, the PSD upon the first time step should be given by (2.5) with μ_0 being equal to $\mu_0(t = 0)$, i.e., the rubbery elastic modulus of the as-cast film. As evident from (2.5), this PSD has a lower cut-off wavevector, $q_{lc,solid}$ (i.e., a characteristic wavevector below which the PSD has negligible amplitude) that fulfills the relation, $\gamma q_{lc,solid}^2 + d^2G(h_0)/h^2 = 3\mu_0/(h_0^3 q_{lc,solid}^2)$.

By applying the same consideration to (2.6), the PSD of the films in the slow dynamic regime should also have a lower cut-off wavevector, q_{lc}, which however is time-varying and fulfills the relation, $\gamma q_{lc}^2 + d^2 G(h_0)/h^2 = 3(\eta_{eff}/2t)/\left(h_0^3 q_{lc}^2\right)$. Such a time variation of q_{lc} has been studied in detail in [58]. From Fig. 2.4, a crossover to the steady state or slow dynamic regime should occur when t reaches the relaxation time τ_r, where $\tau_r \equiv \eta_{eff,0}/\mu_0$. Based on (2.1b) and (2.4b), simple algebra leads to the relation, $\Gamma_q' = \Gamma_q/(1 - \Gamma_q\tau_r)$ [41]. This relation allows for another way of predicting where the crossover in dynamic regimes occurs. Specifically, on reaching the steady state the viscoelastic relaxation rate should become the same as the liquid relaxation rate or $\Gamma_q' \approx \Gamma_q$. Clearly, this condition begins when $\Gamma_q\tau_r \approx -1$ (and establishes as this quantity diminishes) [41], which can be shown to be mathematically equivalent to $\gamma q^2 + d^2 G(h_0)/h^2 = 3\mu_0/(h_0^3 q^2)$ [41] or $q = q_{lc,solid}$ as discussed above. Clearly, the viscous regime $q_{lc}(t)$ equals to $q_{lc,solid}$ at the crossover time τ_r. Taken together, these considerations suggest that the crossover between the rubbery elastic regime and the slow dynamic regime occurs when t exceeds $1/\Gamma_q(q = q_{lc,solid})$, which is the relaxation time of the *liquid* capillary wave mode with $q = q_{lc,solid}$.

Now imagine that μ_0 increases with time. Given (2.4b), this should cause the relaxation rate of the modes Γ_q' to decrease (Fig. 2.6). In that case, the instantaneous experimental time would be shorter than the new relaxation times, so the PSD should be kinetically locked into the current one (namely, the PSD corresponds to a rubbery elastic film with $\mu_0 = \mu_0(t = 0)$.) Based on the above discussion, the PSD becomes able to evolve from the locked-in PSD only after the time t where $q_{lc}(t)$ is equal to $q_{lc,solid}$ of the locked-in PSD. It is easy to see that this happens when $t \sim \eta_{eff,0}/\mu_0(0)$. In other words, $\eta_{eff}(t)$ should maintain the same linear dependence, $\eta_{eff}(t) = 2\mu_0(0)t$ until $t \sim \eta_{eff,0}/\mu_0(0)$, which is observed in Fig. 2.4. This deliberation shows that our measurement would not be able to detect any evolution in the entanglement density of the film, even if it does. Physically, this is because the relaxation rate of the surface modes decreases upon growth of the entanglement

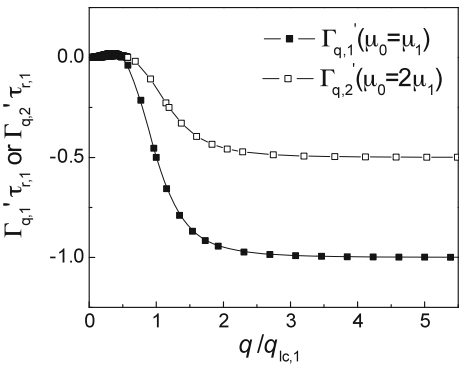

Fig. 2.6 An illustration of the effect of doubling μ_0 on Γ_q'. The *vertical axis* is normalized by $1/\tau_{r,1} \equiv \lim_{q\to\infty} \Gamma_{q,1}'$, the original limiting value before μ_0 is doubled. The *horizontal axis* is normalized by $q_{lc,1}$, the original lower cut-off wavevector of the elastic-state or "rubbery" PSD

density. This causes the rubbery elastic PSD to be locked into the initial one. Only for times exceeding the crossover time for the slow dynamic regime can the PSD grow again.

2.4.2 Residual Stress

In the rapid drying process of spin-coating, it is also speculated that the polymer chains may become compressively deformed [51] besides getting locked into a low entanglement state. Shrinkage of the film upon drying may force the chains into an oblate conformation. This is because the volumetric shrinkage can only take place in the dimension perpendicular to the film, but not the planar dimensions, which are held rigid to the solid substrate [51]. With this, an in-plane residual stress or pre-stress may result [56]. Such a residual stress has been suggested [51] to be responsible for physical aging in as-cast spin-coated polymer films below the T_g [6, 51, 59]. Indeed, large residual stresses ($\sim 10^5$ to $\sim 10^7$ Pa) have been reportedly observed in the dewetting phenomena of PS films supported by a thin liquid layer of polydimethylsilosane (PDMS) [6, 51, 57, 60] or a liquid bath of glycerol [61], surface wrinkling experiments [62, 63] and bending of a polymer-coated micro-cantilever [64].

Vilmin and Raphaël [65], predicted that an in-plane pre-stress in elastic polymer films may cause the occurrence of destabilization analogous to the Asaro-Tiller-Grinfeld instability, well-known in the process of thin film growth by molecular beam epitaxy [66, 67]. In a later publication, Closa, Ziebert and Raphaël discussed in more detail the conditions for this instability [68]. In particular, they showed that, by having surface diffusion in conjunction with a kinematic boundary condition at the free surface, the Asaro-Tiller-Grinfeld instability can occur. But in the absence of surface diffusion, this instability cannot develop, unless if an unphysically large compression (corresponding to an unreasonable stretch ratio λ of >0.03) is applied across the film [68].

In all the systems we studied, including PS-SiO_x, PMMA-SiO_x and poly(α-methyl styrene) on silica, we find that the surface dynamics can be fully accounted for without invoking the Asaro-Tiller-Grinfeld instability. For instance, the calculation of Vilmin and Raphaël in [65] predicts that the growth rates of the unstable capillary wave modes should peak at a characteristic wavevector. But the PSDs found in our measurements (Fig. 2.3) clearly do not show such a characteristic wavevector. We observe that this instability may only exist before the pre-stress is fully relaxed [65], which is found by many experiments to occur within the relaxation time of the elastic regime, as expected [51, 57, 60, 62, 64]. If the instability had ever occurred during our measurement, we should observe a qualitative change in the time variation of η_{eff} before and after the pre-stress relaxes. But the only time-variation we had found of η_{eff} occurs during the PSD stagnant regime (where $\eta_{eff} \sim t$). Stagnancy in the PSD growth clearly cannot result from an act of instability. Therefore we conclude that while a large residual stress is probably

present in our films, it does not play any detectable role in the dynamics we observed. Most probably, the condition for the Asaro-Tiller-Grinfeld instability is not fulfilled in our films.

2.4.3 Chain Adsorption

Recently, a slow adsorption process, in which the polymer chains irreversibly bind to the substrate surface [9–12, 56, 69–71], was also found to contribute to the out-of-equilibrium state of the films. In this subsection, we briefly review the basic features observed of this phenomenon and the out-of-equilibrium properties attributed to this process.

In [9], Fujii et al. observed that upon annealing PS-H-Si and PS-SiO_x (where PS-H-Si denotes PS supported by hydrogen-terminated silicon (H-Si)) at 150 °C, a thin layer of PS formed on the surface of both substrates [9], and could not be removed by rigorous rinsing in toluene—a good solvent of PS. To confirm that this residue layer was formed during annealing by the adsorption of the PS chains to the substrate surface, Fujii et al. measured the thickness of the residue layer, $h_{residue}$, as a function of annealing time. The solid symbols of Fig. 2.7 depict a representative result they obtained. As seen, $h_{residue}$ grows relatively quickly in the first $\sim$20 h, then the growth slows down significantly. Thereafter, $h_{residue}$ continues to grow at the slower rate and reach the steady-state value only after a much later time of $\sim$100 h. Fujii et al. also explored the M_w dependence of the equilibrium thickness of the residue layer, $h_{residue,\infty}$, and found that it scales linearly with the radius of gyration of the polymer, R_g (Fig. 2.8). On fitting their data to the expression, $h_{residue,\infty} = aR_g$, where a is a constant, they found that $a = 0.81$ and 0.47 for H-Si and SiO_x-Si, respectively. This finding illustrates that H-Si is more

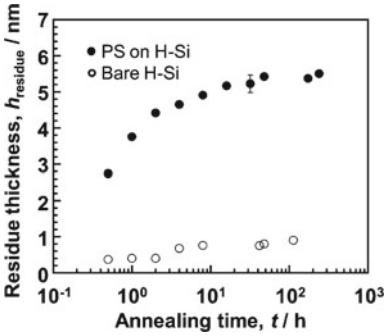

Fig. 2.7 Annealing time dependence of the thickness of the residual film, $h_{residue}$ obtained from PS/H-Si (*solid symbols*) and bare H-Si (*open symbols*). The annealing was carried out at 150 °C in air. The PS has $M_w = 44.1$ kg/mol and initial thickness, $h_0 = 200$ nm (Reproduced with permission from Ref. [33])

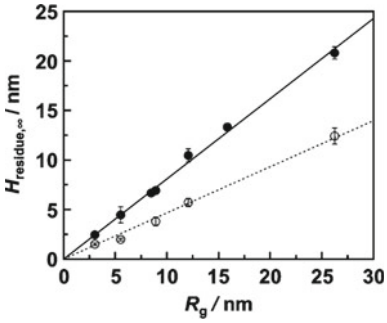

Fig. 2.8 R_g dependence of the equilibrium residue thickness, $h_{residue,\infty}$ for residual films obtained from PS/H-Si (*solid circles*) and PS/SiO_x-Si (*open circles*). In this plot, the value of R_g is deduced from the weight average molecular weight of the polymer (Reproduced with permission from Ref. [33])

attractive to PS than SiO_x is, in keeping with observations that PS-H-Si are more stable against dewetting instability than PS-SiO_x are [9].

In a series of elaborate experiments [10, 69, 70], Napolitano and Wübbenhost showed that the growth of the PS residue layer at an interface upon annealing could lead to measurable change in some physical properties of the films. Specifically, they found that the dielectric relaxation of PS capped between Al electrodes depended on the amount of polymer adsorbed onto the Al electrodes surface. Based on this, they determined that the films might not reach the steady state even upon more than one day of annealing at T_g + 50 °C and the slow relaxation correlated closely with the growth of the adsorbed layer.

In a different experiment performed by the Koga group, using a combination of x-ray reflectivity and AFM imaging [71], it was uncovered that the adsorbed layer formed in PS-H-Si is composed of a high-density inner flattened nanolayer with a surface coverage of ~75 % and a less dense outer layer (Fig. 2.9). In contrast to the thickness of the full adsorbed layer, which, as discussed above, is a fraction of R_g and hence scales with $\sim M_w^{1/2}$ [9], that of the flattened inner layer is independent of M_w and equal to ~2 nm [71]. Based on these observations, Koga et al. proposed that the flattened layer was composed of a tight sequence of polymer trains (Fig. 2.9e) and the outer layer much more loosely packed adsorbed chains grown out from the areas of the substrate not occupied by the flattened layer.

Here, we discuss any discernible influence of the adsorbed layer formation process on our dynamic measurement. As noted above, the viscosity of thick PS-SiO_x with $h_0 > 4R_g$ is the same as bulk viscosity [2]. This shows that the polymer chains constituting the adsorbed layer should make insignificant contribution to the total mobility of the films. In that experiment [2], the steady-state effective viscosity $\eta_{eff,0}$ was established within ~1 h at 150 °C for M_w = 44 to 393 kg/mol. We notice from Fig. 2.7 that this duration is of the same order as the duration of the initial rapid development of the residue film noted above for the same temperature. The fact that the steady-state effective viscosity is established

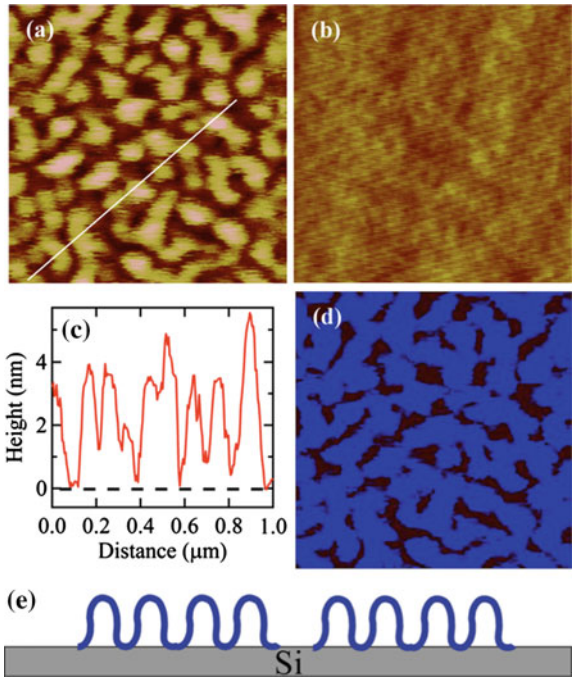

Fig. 2.9 Data and schematic illustrating the structure of the adsorbed layer. **a** AFM topographic image of the flattened inner nanolayer of the PS adsorbed layer left on H-Si after aggressive leaching with chloroform. **b** The full PS adsorbed layer left on H-Si after moderate leaching of ≥5 times with toluene. **c** The cross-sectional profile along the *white line* shown in Panel (**a**). **d** A thresholded image of the image shown in (**a**) with a threshold height value of zero. It shows that the area of the substrate occupied by the flattened layer is $\sim$75 %. **e** Schematic showing the structure of the flattened nanolayer proposed by Jiang et al. [71] (Reproduced with permission from Ref. [71])

[2, 58] even though h_{residue} is still growing suggests that binding of the PS to the substrate surface in the slow-growth phase has little to no effect on the overall mobility of the films [33]. Perhaps this should not be surprising since the adsorbed layer thickness is only a fraction of R_g and hence much smaller than the thickness of these films (which is $h_0 > 4R_g$). For the thinner films, especially those with thickness $< \sim R_g$, the issue warrants further considerations. To address the issue, we study the growth of the adsorbed layer of PS-SiO_x films with various thicknesses h_0 between 3 and 20 nm at an annealing temperature of 120 °C. In this study, the films were annealed for different annealing times then leached in fresh toluene for four or more times. The thickness of the resulting residue film, h_{residue}, was determined by using ellipsometry. The results obtained from the films with M_w = 212 and 940 kg/mol are shown in Fig. 2.10a, b, respectively. As one can see, h_{residue} increases with the initial thickness of the films used to create the adsorbed layer, h_0 (which are specified in the figure legend). This should be contrasted with the above finding that h_{residue} is $\sim R_g$ and independent of h_0. Apparently, the different results

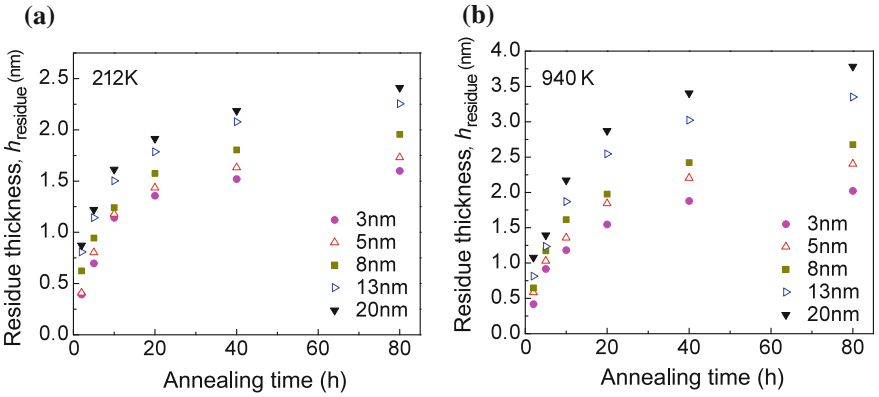

Fig. 2.10 Temporal evolution of $h_{residue}$, the thickness of the adsorbed layer produced from PS spun-cast on silica with various initial thicknesses. **a** Data taken from films with M_w = 212 kg/mol and **b** 940 kg/mol. The annealing temperature was 120 °C. The initial thicknesses are as shown in the legend

are due to the different starting thicknesses h_0 used to create the adsorbed layers. As discussed above for $h_0 > 4R_g$, $h_{residue,\infty} = aR_g$, where $a \sim 0.5$ to 0.8. Therefore, one expects $h_{residue,\infty}$ to depend on h_0 when h_0 is not adequately bigger than R_g [9]. Importantly, Fig. 2.10 shows that the growth of $h_{residue}$ slows down notably after $\sim$20 h for the films with $h_0 \leq 8$ nm and $\sim$40 h for the thicker films. We observe that these times are comparable to the respective times for the η_{eff} measurement to reach the steady-state value (data not shown). This indicates that much of the development of the adsorbed layer occurs during the stagnant PSD regime. As discussed in Sect. 2.4.1, if any structural change in the films associated with the development of the adsorbed layer should cause the growth rate of the surface modes Γ_q' to decrease, the PSD would be locked into the "rubbery elastic" PSD of the as-cast film and our measurement will not be able to detect these changes. This may explain why the chain adsorption process does not seem to have any impact on our PSD measurement.

In light of the slow recovery ($\sim$10 d) observed by Napolitano et al. of the dielectric response of the Al-PS-Al films they studied [10], we perform PSD measurements on some of our PS-SiO_x films for an extensive period of time until rupturing takes place. A representative set of data, taken from a PS-SiO_x film with h_0 = 5 nm and M_w = 393 kg/mol, heated at 120 °C up to 774,000 s or 9 days, is shown in Fig. 2.11. There, one sees that the PSDs fit well to (2.4a) with a single $\eta_{eff,0}$ (= 1.5 × 10^8 Pas) up to t = 253,420 s or 2.9 days. For the PSD taken at a subsequent time of 9 days, (2.4a) clearly underestimates its growth. An examination of the AFM topographic data (Fig. 2.11b) reveals that deep holes were already formed in the film by 9 days of annealing (Fig. 2.11c, d). Since (2.4a) is based on linear analyses, the poor agreement between (2.4a) and the respective PSD is understood to be due to violation of the linear approximation.

Constancy of the measured $\eta_{eff,0}$ up to the time when holes begins to form in the film strongly suggests that our measurement of the steady-state effective viscosity in *thin* films, same as for thick films ($h_0 > 4R_g$), is not visibly affected by the development of the adsorbed layer in the slow dynamic regime. It follows that $\eta_{eff,0}$ can be used as a measure of the film stability. The bigger $\eta_{eff,0}$ is, the more long-lived the film should be. For the 5 nm, 393 kg/mol film considered above (Fig. 2.11), the measured $\eta_{eff,0}$ (i.e., 1.5×10^8 Pas) is $\sim$1/100 times the bulk value, indicating that this film is much less stable than thick films. A preliminary result shows that when the film is deposited on H-Si, the value of $\eta_{eff,0}$ increases by a factor of 2–3. This implies that by depositing polymer films on a substrate surface that adsorbs the polymer chains more, the lifetime of the films can be improved. Further investigations are warranted to explore to what extent the stability of a film can be improved by using this approached.

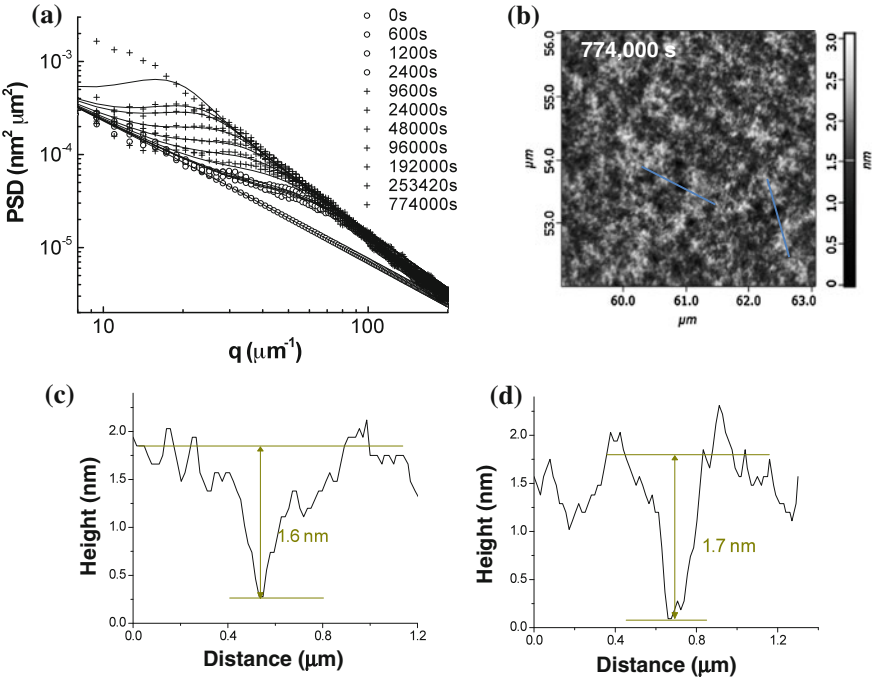

Fig. 2.11 Surface topographic data of a 5 nm, 393 kg/mol PS film upon extensive annealing at 120 °C. **a** The power spectral density found at various times as shown in the legend. The *symbols* denote the experimental data. The *solid lines* are model lines obtained by fitting the $t \leq 253420$ s data to (2.4a). The fitted value of $\eta_{eff,0}$ ($\equiv M_{tot}/3\ h_0^3$) = 1.5×10^8 Pas is $\sim$1/140 times the bulk value. The film maintains this anomalously low viscosity until after 253,420 s (or 2.9 days), whereupon further annealing brought about deep holes with depth $\approx 0.3\ h_0$ as seen in the AFM topographic image displayed in panel **b** and the cross-sectional profiles in panels **c–d**

2.5 Conclusion

In conclusion, issues concerning the out-of-equilibrium properties of spin-coated polymer films are both academically challenging and of practical importance. An important, but relatively little discussed out-of-equilibrium attribute of spin-coated polymer films is their thickness uniformity. Because the films are smoother than equilibrium, they roughen on heating. Our studies show that the equilibrium pathway of the film surface is governed by the dynamics of the surface capillary wave modes, which in turn can be characterized by the total mobility, or equivalently effective viscosity of the films. For entangled polymer films that are viscoelastic, model analysis of the experimental data allows for additional determination of the shear modulus of the as-cast films. By using the information gathered from PS-SiOx films with a broad range of M_w and h_0 at various temperatures, we addressed several out-of-equilibrium phenomena commonly attributed to as-cast polymer films, including reduced chain entanglement, residual stress and irreversible chain adsorption to the substrate surface. Our measurement shows that the shear modulus of the as-cast films is typically $\sim 1/10$ the equilibrium bulk value. On the other hand, the effective viscosity of the same films (for those with $h_0 > 4R_g$) may reach a steady-state value that agrees with bulk viscosity. A simple interpretation would be that the as-cast films have a reduction in the density of entanglement, but upon heating the density of entanglement regains the equilibrium value. As for residual stress, although numerous experiments support its presence in thin films, we do not notice any influence on our measurement. This observation, however, may not be surprising as existing theory shows that residual stress may not produce instability in a film if there is no surface diffusion. We surmise that surface diffusion may be suppressed in high-M_w films. Various experiments had found that the surface mobile regime is several nanometers thick. So for the films with sufficiently high M_w, the surface chains may be partially embedded in the slower inner region and so have a lessened mobility. Finally for chain adsorption on the substrate surface, we also do not observe any noticeable influence on our measurement. For the thick films with thickness much larger than R_g, effects of the adsorbed layer are expected to be inconsequential due to its relatively insignificant thickness. For the films with thickness comparable to R_g, our residue thickness versus annealing time measurement indicates that the majority of the development of the adsorbed layer occurs before the steady-state effective viscosity is established. Apparently, the subsequent, minor development of the adsorbed layer has negligible effect on the steady-state effective viscosity.

Acknowledgments We acknowledge important contribution from Prof. Chi-Hang Lam in the development of the model analyses discussed in this chapter. Contributions from former members of the group, particularly Dr. Andrew Clough, Dr. Yoshihisa Fujii, Dr. Ranxing N. Li and Dr. Dongdong Peng are also acknowledged. We are thankful to the support of National Science Foundation through the projects DMR-0706096, DMR-0908651, DMR-1004648 and DMR-1310536, which have enabled the results discussed in this chapter.

References

1. Reiter, G., de Gennes, P.-G.: Eur. Phys. J. E **6**, 25 (2001)
2. Tsui, O.K.C., Wang, Y.J., Lee, F.K., Lam, C.H., Yang, Z.: Macromolecules **41**, 1465 (2008)
3. Orts, W.J., Vanzanten, J.H., Wu, W.L., Satija, S.K.: Phys. Rev. Lett. **71**, 867 (1993)
4. Mukherjee, M., Bhattacharya, M., Sanyal, M.K., Geue, T., Grenzer, J., Pietsch, U.: Phys. Rev. E **66**, 061801 (2002)
5. Miyazaki, T., Nishida, K., Kanaya, T.: Phys. Rev. E **69**, 022801 (2004)
6. Reiter, G., Hamieh, M., Damman, P., Sclavons, S., Gabriele, S., Vilmin, T., Raphael, E.: Nat. Mater. **4**, 754 (2005)
7. Vilmin, T., Raphael, E.: Europhys. Lett. **72**, 781 (2005)
8. Vilmin, T., Raphael, E.: Eur. Phys. J. E **21**, 161 (2006)
9. Fujii, Y., Yang, Z., Leach, J., Atarashi, H., Tanaka, K., Tsui, O.K.C.: Macromolecules **42**, 7418 (2009)
10. Napolitano, S., Wubbenhorst, M.: Nat. Commun. **2**, 260 (2011)
11. Housmans, C., Sferrazza, M., Napolitano, S.: Macromolecules **47**, 3390 (2014)
12. Koga, T., Jiang, N., Gin, P., Endoh, M.K., Narayanan, S., Lurio, L.B., Sinha, S.K.: Phys. Rev. Lett. **107**, 225901 (2011)
13. Jiang, N.S., Shang, J., Di, X.Y., Endoh, M.K., Koga, T.: Macromolecules **47**, 2682 (2014)
14. Chen, F., Lam, C.-H., Tsui, O.K.C.: Science **343**, 975 (2014)
15. Wang, Y.J., Lam, C.H., Zhang, X., Tsui, O.K.C.: Eur. Phys. J. **141**, 181 (2007). (Special Topics)
16. Wang, Y.J., Tsui, O.K.C.: Langmuir **22**, 1959 (2006)
17. Wang, Y.J., Tsui, O.K.C.: J. Non-Cryst. Solids **352**, 4977 (2006)
18. Yang, Z., Lam, C.-H., DiMasi, E., Bouet, N., Jordan-Sweet, J., Tsui, O.K.C.: Appl. Phys. Lett. **94**, 251906 (2009)
19. Kajiyama, T., Tanaka, K., Takahara, A.: Macromolecules **30**, 280 (1997)
20. Tsui, O.K.C., Wang, X.P., Ho, J.Y.L., Ng, T.K., Xiao, X.D.: Macromolecules **33**, 4198 (2000)
21. Wang, X.P., Xiao, X.D., Tsui, O.K.C.: Macromolecules **34**, 4180 (2001)
22. Du, B.Y., Tsui, O.K.C., Zhang, Q.L., He, T.B.: Langmuir **17**, 3286 (2001)
23. Dubourg, F., Aime, J.P., Marsaudon, S., Couturier, G., Boisgard, R.: J. Phys.: Condens. Matter **15**, 6167 (2003)
24. Valignat, M.P., Oshanin, G., Villette, S., Cazabat, A.M., Moreau, M.: Phys. Rev. Lett. **80**, 5377 (1998)
25. Manias, E., Chen, H., Krishnamoorti, R., Genzer, J., Kramer, E.J., Giannelis, E.P.: Macromolecules **33**, 7955 (2000)
26. Reiter, G.: Phys. Rev. Lett. **87**, 186101 (2001)
27. Damman, P., Gabriele, S., Sclavons, S., Desprez, S., Villers, D., Vilmin, T., Raphael, E., Hamieh, M., Alakhrass, S., Reiter, G.: Phys. Rev. Lett. **99**, 036101 (2007)
28. Shin, K., Obukhov, S., Chen, J.-T., Huh, J., Hwang, Y., Mok, S., Dobriyal, P., Thiyagarajan, P., Russell, T.P.: Nat. Mater. **6**, 961 (2007)
29. Heslot, F., Fraysse, N., Cazabat, A.M.: Nature **338**, 640 (1989)
30. Yang, Z., Fujii, Y., Lee, F.K., Lam, C.-H., Tsui, O.K.C.: Science **328**, 1676 (2010)
31. Lam, C.-H., Tsui, O.K.C., Peng, D.: Langmuir **28**, 10217 (2012)
32. Kim, H., Ruhm, A., Lurio, L.B., Basu, J.K., Lal, J., Lumma, D., Mochrie, S.G.J., Sinha, S.K.: Phys. Rev. Lett. **90**, 068302 (2003)
33. Li, C.H., Koga, T., Jiang, J., Sharma, S., Narayanan, S., Lurio, L.B., Hu, Y., Jiao, X., Sinha, S. K., Billet, S., Sosnowik, D., Kim, H., Sokolov, J.C., Rafailovich, M.H.: Macromolecules **38**, 5144 (2005)
34. Wang, S.-F., Yang, S., Lee, J., Akgun, B., Wu, D.T., Foster, M.D.: Phys. Rev. Lett. **111**, 068303 (2013)
35. Chai, Y., Salez, T., McGraw, J.D., Benzaquen, M., Dalnoki-Veress, K., Raphael, E., Forrest, J. A.: Science **343**, 994 (2014)

36. McGraw, J.D., Salez, T., Baeumchen, O., Raphael, E., Dalnoki-Veress, K.: Phys. Rev. Lett. **109**, 128303 (2012)
37. Zhu, L., Brian, C.W., Swallen, S.F., Straus, P.T., Ediger, M.D., Yu, L.: Phys. Rev. Lett. **106**, 256103 (2011)
38. Vrij, A., Overbeek, J.T.: J. Am. Chem. Soc. **90**, 3074 (1968)
39. Yang, Z., Peng, D., Clough, A., Lam, C.H., Tsui, O.K.C.: Eur. Phys. J. **189**, 155 (2010). (Special Topics)
40. Yang, Z., Clough, A., Lam, C.-H., Tsui, O.K.C.: Macromolecules **44**, 8294 (2011)
41. Peng, D., Yang, Z., Tsui, O.K.C.: Macromolecules **44**, 7460 (2011)
42. Hiemenz, P.C., Lodge, T.P.: Polymer Chemistry, 2nd edn. Marcel Dekker Inc, New York (1984)
43. Yang, Z., Fujii, Y., Lee, F.K., Lam, C.-H., Tsui, O.K.C.: Science **328**, 1676 (2010)
44. Paeng, K., Ediger, M.D.: Macromolecules **44**, 7034 (2011)
45. Peng, D., Li, R.N., Lam, C.-H., Tsui, O.K.C.: Chin. J. Polym. Sci. **31**, 12 (2013)
46. Lam, C.-H., Tsui, O.K.C.: Phys. Rev. E **88**, 042604 (2013)
47. Li, R.N., Chen, F., Lam, C.-H., Tsui, O.K.C.: Macromolecules **46**, 7889 (2013)
48. Yang, Z., Clough, A., Lam, C.-H., Tsui, O.K.C.: Macromolecules **44**, 8294 (2011)
49. Fredrickson, G.H., Ajdari, A., Leibler, L., Carton, J.P.: Macromolecules **25**, 2882 (1992)
50. Safran, S.A., Klein, J.: J. Phys. II Fr. **3**, 749 (1993)
51. Raegen, A., Chowdhury, M., Calers, C., Schmatulla, A., Steiner, U., Reiter, G.: Phys. Rev. Lett. **105**(22), 227801 (2010)
52. Barbero, D.R., Steiner, U.: Phys. Rev. Lett. **102**, 248303 (2009)
53. Fetters, L.J., Lohse, D.J., Milner, S.T.: Macromolecules **32**, 6847 (1999)
54. Rubinstein, M., Colby, R.H.: Polymer Physics, 1st edn. Oxford University Press, New York (2003)
55. Strobl, G.R.: The Physics of Polymers. Springer, Berlin (1996)
56. Li, R.N., Clough, A., Yang, Z., Tsui, O.K.C.: Macromolecules **45**, 1085 (2012)
57. Damman, P., Gabriele, S., Coppee, S., Desprez, S., Villers, D., Vilmin, T., Raphael, E., Hamieh, M., Al Akhrass, S., Reiter, G.: Phys. Rev. Lett. **99**, 036101 (2007)
58. Yang, Z.H., Wang, Y., Todorova, L., Tsui, O.K.C.: Macromolecules **41**, 8785 (2008)
59. Priestley, R.D., Ellison, C.J., Broadbelt, L.J., Torkelson, J.M.: Science **309**, 456 (2005)
60. Chowdhury, M., Freyberg, P., Ziebert, F., Yang, A.C.M., Steiner, U., Reiter, G.: Phys. Rev. Lett. **109**, 136102 (2012)
61. Bodiguel, H., Fretigny, C.: Eur. Phys. J. E **19**, 185 (2006)
62. Chung, J.Y., Chastek, T.Q., Fasolka, M.J., Ro, H.W., Stafford, C.M.: ACS Nano **3**, 844 (2009)
63. Chung, J.Y., Nolte, A.J., Stafford, C.M.: Adv. Mater. **23**, 349 (2011)
64. Thomas, K.R., Steiner, U.: Soft Matter **7**, 7839 (2011)
65. Vilmin, T., Raphael, E.: Phys. Rev. Lett. **97**, 036105 (2006)
66. Asaro, R.J., Tiller, W.A.: Metall. Trans. **3**, 1789 (1972)
67. Grinfeld, M.A.: J. Nonlinear Sci. **3**, 35 (1993)
68. Closa, F., Ziebert, F., Raphael, E.: Phys. Rev. E **83**, 051603 (2011)
69. Napolitano, S., Capponi, S., Vanroy, B.: Eur. Phys. J. E **36**, 61 (2013)
70. Napolitano, S., Rotella, C., Wubbenhorst, M.: ACS Macro Lett. **1**, 1189 (2012)
71. Jiang, N., Shang, J., Di, X., Endoh, M.K., Koga, T.: Macromolecules **27**, 2682 (2014)

http://www.springer.com/978-3-319-21947-9

Non-equilibrium Phenomena in Confined Soft Matter
Irreversible Adsorption, Physical Aging and Glass Transition at the Nanoscale
Napolitano, S. (Ed.)
2015, VIII, 300 p. 131 illus., 71 illus. in color., Hardcover
ISBN: 978-3-319-21947-9